EPSC Abstracts
Vol. 13, EPSC-DPS2019-1705-1, 2019
EPSC-DPS Joint Meeting 2019

EPSC
EPSC-DPS Joint Meeting 2019
15–20 September 2019 | Geneva, Switzerland

Correlating Radar and Visible Stratigraphic Records in the Martian North Polar Layered Deposits

P. Becerra (1), D. Nunes (2), I. Smith (3), M.M. Sori (4), Y. Brouet (1), N. Thomas (1)
(1) Physikalisches Institut, Universität Bern, Switzerland (patricio.becerra@space.unibe.ch) (2) Jet Propulsion Laboratory, Pasadena, California, USA (3) York University, Toronto, Ontario, Canada. (4) University of Arizona, Tucson, AZ, USA.

Abstract

We present a preliminary correlation of visible imagery and stereo-topography from HiRISE with sub-surface radar from SHARAD of Mars' NPLD.

1. Introduction

A long-standing problem in Mars Polar Science is the interpretation of the stratigraphic record preserved in Mars' icy North Polar Layered Deposits (NPLD) [1] (Fig. 1a), whose accumulation patterns of ice and dust are associated with recent climatic changes forced by variations in the planet's astronomical parameters [2]. The internal bedding is visible from orbit in exposures within spiraling troughs that dissect the NPLD dome (Fig. 1a,b). Studies have used images of these troughs to map the stratigraphy [3-6] and describe links between NPLD accumulation and astronomical forcing [7-10]. Sub-surface radar sounding also observes this internal structure. The Shallow Radar (SHARAD) [11] detects changes in dielectric properties with depth. As these vary for layers with different amounts of dust, layering is observed as "reflector" surfaces [12].

The optical and radar-based stratigraphies have predominantly been studied in isolation. In terrestrial climate science [13], orbital climate forcing was confirmed by correlation of sedimentary, geochemical and paleo-magnetic records, suggesting that integration of datasets is key to understanding the record in the NPLD. In general, both radar and optical layers are assumed to result from varying amounts of dust in the ice [14,15], but differences in vertical resolution have prevented 1-to-1 correlation.

Here, we test the hypothesis that highly protruding 'Marker Beds (MBs)' have sufficient dielectric contrast with neighboring beds to create radar reflections. If true, this would associate individual reflectors to exposed beds, allowing for dust/ice columns based on the combined data, which could constrain orbitally-forced accumulation models [16,17] to decipher the climate record of the NPLD.

2. Methods

Becerra et al. [8] mapped the stratigraphy of the NPLD by identifying sequences of MBs in "protrusion profiles" of bed exposures in troughs made from HiRISE [18] Digital Terrain Models (DTMs; [19]), and correlating these from different locations (Fig. 1; [8]). A protrusion profile for site N0 is shown in Fig. 2a. With these data, our approach to correlation is a 4-step process:

(1) *Average SHARAD data near the exposures to obtain representative radargrams.* The variability of the SHARAD response within small regions of interest (ROIs) next to exposure sites is not negligible. To assess this, we selected segments of three SHARAD radar tracks that fall within a 3 km ROI near a study site, and averaged all soundings in each segment (Fig. 2b,c). This is representative of the variations in radar response within the ROI.

(2) *Compare average radargrams directly to the protrusion profiles of* [8] *to search for an MB-reflector correlation*. For this, we subtract the linear attenuation in the data and normalize all quantities to mean = 0 and variance = 1. We then search for the maximum cross-correlation between protrusion profiles and average radargrams.

(3) *Model the radar wave propagation* [14] *through synthetic permittivity (ε) profiles,* which would be constrained by the best-fit correlations from step 2. MBs would translate into layers of varying ε depending on their initial correlation with the radargram. We would then compare the model radargrams to the real ones at each location. We tested a preliminary model, selecting specific MBs from the N0 profile and assigning them ε = 4 over a water ice background with ε = 3.12. Fig. 3 shows the dielectric profile modeled after the protrusion profile of site N0, and the resulting simulated radargram.

(4) *Correlate the simulated radargrams to real SHARAD data using spectral analysis and pattern-matching algorithms.* This correlation will result in representative HiRISE/SHARAD-based stratigraphic columns of ε, which can be transformed to fractional dust-content [20,21] that can serve as virtual ice cores and be used to constrain accumulation models.

3. Preliminary Results

Results of the cross-correlation of SHARAD with the protrusion profiles for sites N0, N2, and N11 are

shown in Fig 4. For the direct cross-correlation with protrusion we select only the sections of the radargrams that correspond to the estimated relevant depth range [2–8 μs]. For N0, we also ran a comparison with the preliminary model results, which includes the surface reflection and an "overburden" [0–8 μs]. The greyed-out portions of Fig. 4 represent the shift applied to the protrusion profile according to the best-fit lag from the cross-correlation. A smaller lag is better, provided that the match between reflectors and protrusion is sensible. N2 and N11 show equally good matches, better than N0 (Fig. 4a). Some peaks in the radargram match troughs in protrusion instead. However, radar reflections represent interfaces between materials of different ε, thus, it is not implausible that a transition to a low-dust, less-protruding layer would also produce a relatively strong reflection. The protrusion-based model for N0 shows an acceptable preliminary cross-correlation with the real radargram (Fig. 4b).

4. Conclusions and Future Work

Beds of high protrusion appear to match radar reflectors at three sites, and preliminary results from the model are positive showing that this method is the correct approach to this problem. An attempted correlation at site N6 failed at the first stage however. We must study all geometrically favourable locations and test for statistical significance at each one. In addition, we will use the correlations with protrusion to inform the model and then use Dynamic Time Warping [7,22] to tune the model and find the best-fit dielectric profile at each site. The final step of the work will be to transform these profiles into dust/ice ratio columns [20,21] for use as input on accumulation models [17]. Naturally, a higher spatial-resolution radar in orbit around Mars would greatly improve the chances of subsurface-surface integration. Such an instrument is being proposed as a NASA Discovery mission [23], and this work can help predict the results that would be returned.

5. Figures

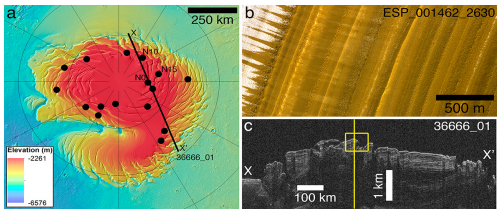

Figure 1. (a) MOLA map of the NPLD. Dots = study sites [6] with HiRISE DTMs. Line = ground track of the SHARAD radargram in (c). **(b)** HiRISE image of exposed layers in an NPLD trough. **(c)** SHARAD radargram (X-X' in 1a). Yellow square = location of site N0. Line = position of the profiles of Fig. 2.

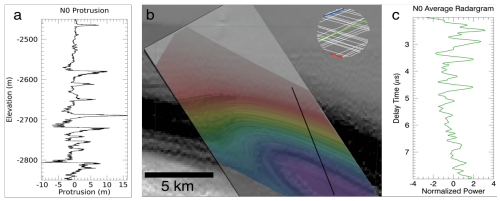

Figure 2. (a) Protrusion profile of N0. **(b)** Zoom view of site N0 showing trough and HiRISE colorized elevation DTM draped over MOLA topography. ROI for radargram averaging in top right. Black diagonal line = track of the protrusion profile. **(c)** Average of individual radar soundings along the green track shown in ROI.

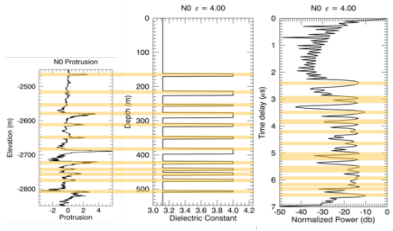

Figure 3. N0 protrusion profile (left) used to build a dielectric profile (center), through which a model radar wave is propagated to obtain a simulated radargram (right).

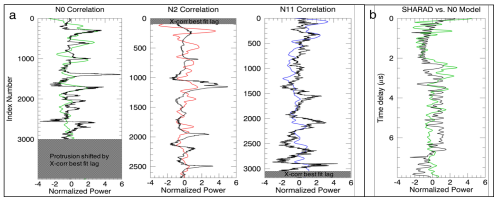

Figure 4. (a) Direct cross-correlation of average radargrams with protrusion **(b)** Cross-correlation of simulated N0 radargram with real radargram.

References

[1] Smith, et al. *Icarus* (2017) [2] Cutts, et al. *Science* (1976) [3] Fishbaugh et al. (2006) [4] Fishbaugh et al. *GRL* (2010) [5] Limaye et al. *JGR* (2012) [6] Becerra et al. *JGR* (2016) [7] Laskar et al. *Nature* (2002) [8] Milkovich and Head, *JGR* (2005) [9] Perron and Huybers, *Geology* (2009) [10] Becerra et al. *GRL* (2017) [11] Seu et al. *JGR* (2007) [12] Putzig et al. *Icarus* (2009) [13] Imbrie, *Icarus* (1982) [14] Nunes & Phillips, *JGR* (2006) [15] Christian, et al. *Icarus* (2013) [16] Levrard et al. JGR (2007) [17] Hvidberg et al. *Icarus* (2012) [18] McEwen et al. JGR (2007) [19] Kirk et al. JGR (2008) [20] Stillman, et al. *J.Phys.Chem.* (2010) [21] Brouet et al. *Icarus* (2018) [22] Sori et al. Icarus (2014). [23] Byrne et al. *this conference*